High-Resolution Post-Earthquake Recovery Simulation: Impact of Safety Cordons

Earthquake Spectra
XX(X):2–31

DOI: 10.1177/87552930221075364
www.sagepub.com/
SAGE

Anne M. Hulsey,[1] M.EERI, Jack W. Baker,[2] M.EERI, and Gregory G. Deierlein,[2] M.EERI

Abstract

A framework is proposed to assess the impact of safety cordons on the recovery of community functions after an earthquake, using high-resolution geospatial information to simulate the damage, cordons, and recovery trajectories for buildings in the affected area. Ground motion maps are developed to characterize shaking intensities for regional building-level engineering assessments of damage, repair times, and recovery times to quantify the impact of access restrictions associated with cordons around tall buildings with impaired collapse safety. The results are presented as recovery curves that quantify the cumulative loss in building functionality across the community as a function of time following an earthquake. A case study considers recovery of office space in downtown San Francisco, following a $M_w 7.2$ event on the San Andreas Fault. For this scenario, an average of 219 community days of office functionality are lost in the first year, representing about 60% of the total office space capacity. About one-third of the loss is attributed to access restrictions associated with cordons around older tall buildings. The proposed framework can be used to investigate the efficacy of various mitigation strategies to expedite recovery. While the most effective strategy for mitigating the overall impact of cordon restrictions is to seismically retrofit older tall buildings that trigger cordons, other less expensive preparedness measures are shown to be effective, depending on the recovery time frame of interest. Specifically, recovery preparedness measures are generally more effective when evaluated for longer-term recovery targets (e.g., recovery of function after 12 months) as compared to short-term targets (e.g., recovery after 4 months).

Keywords

Post-earthquake safety cordons, building functional recovery time, community resilience, recovery targets, mitigation strategies, San Francisco, FEMA P-58, REDi, regional ground motion simulation

Introduction

A key component of community resilience is the ability to recover critical community functions after a large earthquake. The U.S. federal government's Community Resilience Planning Guide for Buildings and Infrastructure Systems (NIST 2016) cites several categories of community capital (e.g. the financial, built, social, cultural capitals, etc.), while focusing on the built environment's role in supporting the other types of capital. For example, a functioning built environment would allow residents to stay in their homes, grocery stores to provide access to food, and governments to coordinate the recovery efforts. The Planning Guide describes how communities can identify their critical functions, set recovery time targets for various hazard levels, and assess the gap between the anticipated and the desired performance. This conceptual framework of pairing community functions with associated time targets was pioneered in *The Resilient City: Defining What San Francisco Needs From its Seismic Mitigation Policies* (SPUR 2009). Figure 1a shows a subset of the *Resilient City*'s recovery targets (blue diamonds) and the anticipated performance (black Xs), highlighting the gap between the city's resilience goals and the status quo.

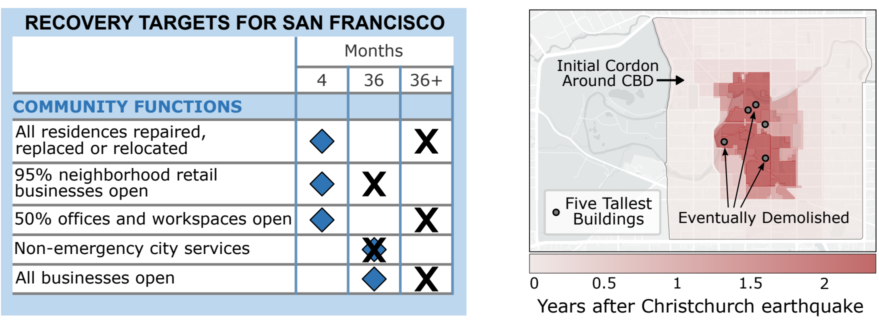

(a) (b)

Figure 1. (a) Examples of the target (blue diamonds) versus expected (black X's) recovery time frames for San Francisco's community functions (adapted from SPUR 2009).
(b) Duration of access restrictions in the Central Business District (CBD) due to cordons after the 2011 Christchurch earthquake, shown in relation to the five tallest buildings (17 to 23 stories), three of which were eventually demolished. Geospatial data from CERA (2016).

[1] Department of Civil and Environmental Engineering, The University of Auckland, Auckland, New Zealand
[2] Department of Civil and Environmental Engineering, Stanford University, Stanford, CA, USA

Corresponding author:
Anne Hulsey: anne.hulsey@auckland.ac.nz

When considering the performance of a dense urban downtown area, it is important to recognize the potential for widespread access restrictions due to post-earthquake safety cordons (hereafter, cordons). Cordons restrict access into potentially dangerous zones, preventing casualties in the event of an aftershock by inhibiting the zone's pre-earthquake community functions (Shrestha et al. 2021). The February 2011 Canterbury earthquake in Christchurch, New Zealand demonstrated the potential scale and political/legal challenges of this issue, with cordons restricting access to the Central Business District (CBD) for many months after the earthquake (Chang et al. 2014; Marquis et al. 2017; Underwood et al. 2020). The damage was so extensive that the initial cordons encompassed the entire CBD (light pink in Figure 1b). The most prolonged access restrictions (over two years, shown in dark red) were driven by heavily damaged buildings with impaired collapse safety, requiring extensive repairs or demolition. Cordons around damaged tall buildings were particularly disruptive, due to both the larger "fall zone", which could be impacted by debris, and the logistics of stabilizing a larger structure. (Note that Christchurch's tallest building was $87m$ tall, while $75m$ is the lower bound for San Francisco's Tall Building Inventory.) (ATC-119 2018) In addition to the direct impacts on building repairs and reconstruction, the cordon also affected other recovery-related decisions, such as whether individual businesses would return to the CBD or relocate entirely.

While the Christchurch CBD is the best documented example of cordons in a dense urban area, similar situations have occurred after other earthquakes. Examples include the city center in L'Aquila, Italy, cordoned following the earthquake in 2009 (Contreras et al. 2014), and cordons around damaged buildings following the 1989 Loma Prieta, 2010 Maule, and 2017 Puebla-Morelos earthquakes (Shepard et al. 1990; Miranda 2020). While there are photographic and anecdotal reports of past cordons, there have generally not been systematic efforts to document and map the cordon management. For example, cordons were not mentioned in a comprehensive reconnaissance report for the 2010 Maule earthquake (EERI 2010) or other detailed reports of damage to tall buildings (Rojas et al. 2011; Naeim et al. 2011; Carpenter et al. 2011). However, some of the buildings referenced are known to have had cordons, such as Torre O'Higgins in Concepción (Miranda 2020). These examples point to a general lack of attention given to cordons and their impact on recovery.

The long and unprecedented access restrictions in Christchurch demonstrate the potential for cordons to significantly disrupt recovery in dense downtown areas. The city of San Francisco has recognized this, highlighting the need for protocols and procedures for establishing cordons around damaged buildings, as well as recovery plans for individual tall buildings and the financial district as a whole (ATC-119 2018). Accordingly, post-earthquake recovery assessments and plans should consider the impacts of cordons around buildings with impaired collapse safety, including access restrictions for otherwise undamaged buildings and delayed repairs for those that are damaged. In the absence of empirical evidence from past earthquakes, the proposed framework combines performance-based earthquake engineering simulations with modeling assumptions for how cordons may affect the neighboring buildings' functional recovery time. These assumptions can be refined as future earthquake reconnaissance efforts collect new data on cordons.

The proposed framework relies on a systematic performance-based approach to integrate building- and community-level assessments. The following sections outline how the framework uses state of the art building-level assessment tools to quantify community-level recovery over time. The results for individual buildings are integrated into geospatial analyses of the community, considering both geographically distributed ground shaking intensities and access restrictions around damaged tall buildings. Details of the framework are described and demonstrated through a case study to illustrate how the analyses can be used to evaluate the efficacy of various mitigation strategies for achieving resilience targets.

Performance-Based Earthquake Engineering

Performance-Based Earthquake Engineering (PBEE) focuses on quantifying how a system (e.g. a building or a community) will perform during an earthquake. The PBEE framework captures a system's response and the associated consequences in distinct steps, with each conditioned on the previous: ground shaking, the system's physical response, damage, and consequences (Moehle and Deierlein 2004). The following sections describe this process at the community- and building-levels, highlighting features that will be used in the proposed framework.

Community-level PBEE

A community performance assessment begins with the built environment's response to ground shaking. Whereas assessments for individual assets only consider the shaking at a single location, a community assessment must incorporate the shaking that occurs across the region. This is often based on a scenario earthquake, using a map of ground motion intensities at geographically distributed sites. For example, the recent HayWired Scenario (Wein and Detweiler 2018) evaluated how the San Francisco Bay Area may be affected by ground motion intensities that were based on one simulated realization of a $M_w 7.0$ earthquake on the Hayward Fault. While single earthquake realizations can be useful to illustrate and raise awareness of what may happen to a community, a single realization does not capture the range of potential results, which is important for more rigorous planning decisions (Wesson and Perkins 2001; Lee and Kiremidjian 2007; Adachi and Ellingwood 2009; Jayaram and Baker 2010). Therefore, the proposed framework employs a suite of ground motion maps, considering multiple earthquake realizations, to account for the uncertainty in shaking intensities that may be experienced due to a scenario earthquake. It is possible to further extend the analyses to probabilistically include many earthquake scenarios; however, in keeping with resilience planning guidance, this framework focuses on recovery targets for distinct earthquake scenarios, rather than the fully probabilistic hazard.

A second important feature of community-level PBEE is how the built environment is modeled. The built environment encompasses both buildings and infrastructure (NIST 2021), yet there are trade-offs in deciding which assets to consider in the model.

Decisions regarding the model complexity and level of resolution will be informed by the type of questions the study aims to address. While the proposed framework can, in concept, include both buildings and infrastructure, this literature review and the ensuing case study focus only on modeling the community's buildings.

Many regional studies (including HayWired) rely on FEMA's Hazus software (FEMA 2012a) for estimating building repair cost, casualties, and population displacement across a community. The Hazus methodology uses spatial aggregation to assess portfolios of buildings, rather than each individual building. By creating a portfolio for each census tract (based on the total number of buildings in each structural type and occupancy category), the collective results can be based on the expected performance of simple, generic building vulnerability models. While this level of resolution is useful for aggregated data, such as the total building repair cost for the census tract, it cannot capture the local impact of individual damaged buildings.

Cimellaro et al. (2018) used the generic Hazus building models at the individual building resolution to consider the impact of building debris on access to roadways and buildings. Their study employed Hazus models to estimate the volume of debris, based on the building damage states, which was further assumed to affect the functionality of nearby roads. Similar to the proposed framework, Cimellaro et al.'s study looked beyond the simple aggregation of individual building performances by considering the collective impacts that arise at the community level. However, Cimellaro et al.'s study only considered the expected performance and relied on simplified assumptions for the volume and impact of debris. In contrast, the proposed framework uses more detailed building models to simulate the potential range of performance and identify damage that would require a cordon around a building. Paired with ground motion maps to quantify the variability in ground shaking, the proposed approach provides a distribution of potential outcomes, ranging from cases with very few cordons to others with access restrictions across most of the community.

Burton et al. (2016)'s community resilience assessment framework also used a combination of multiple realizations of ground motions and detailed building models to simulate building performance. Their study employed Monte Carlo simulation to model realizations of community performance, sampling each building's functionality state from fragility curves derived from component-level damage modeling. Burton et al. (2017) subsequently applied the methodology in a case study of a residential community in India, including the impact of recovery delays due to resource demand surge, based on the number of buildings needing repairs (Comerio 2006). This secondary impact of widespread damage highlights the importance of including the full variability when assessing community performance. The proposed framework employs similar methods for incorporating variability in building performance and recovery delays due to cordons.

Building-level PBEE

FEMA P-58 (FEMA 2012b) is a state of the art methodology for implementing PBEE at the individual building level, developed from previous efforts as reviewed by Mieler and Mitrani-Reiser (2018). The performance assessment simulates many realizations of consequences (decision variables, DV) based on damage to structural and non-structural components (damage measures, DM) that are distributed throughout the building. The damage is based on the building response over the height of the building (engineering demand parameters, EDP) conditioned on the level of shaking (intensity measure, IM). This detailed, component-level simulation provides insight into the variability of the consequences. For example, several research studies have quantified the relationship between damage measures and increased probability of collapse, for the purpose of post-earthquake building evaluation (e.g., Raghunandan et al. 2015; Burton and Deierlein 2018; Hulsey 2020; Deierlein et al. 2020). Damage to tall buildings could endanger pedestrians and neighboring buildings, due to both an increased probability of collapse and damage to heavy exterior cladding that could fall from upper stories. The proposed framework is designed to assess the likelihood of cordons based on each building's simulated response and damage.

The REDi Rating System (Almufti and Willford 2013) builds on the FEMA P-58 methodology to provide refined estimates of building downtime. The cumulative repair time is based on a logical repair sequence, considering the type of components that are damaged (e.g., structural system, interior partitions, exterior cladding, etc.) and whether the severity of damage would hinder re-occupancy, functional recovery, or full recovery. In addition to calculating the repair time for each recovery state, REDi considers so-called impeding factors that must be resolved before repairs can begin (Comerio 2006), including the estimated times required for damage inspection, financing (e.g. collecting insurance payments or procuring loans), engineering design/permitting, and contractor mobilization. (These impeding factors durations are sampled from probability distributions, solicited via expert judgment for the United States, considering recovery following a design level earthquake. Other hazard levels or locations may warrant adjustments to these distributions.) According to REDi's impeding factor framework, once the damage inspection is complete, the other three factors (financing, engineering design/permitting, and contractor mobilization) are addressed in parallel, such that the repairs are initiated as soon as the longest impeding factor is resolved. The proposed framework extends REDi's impeding factor model to include the additional delays in building repairs due to access restrictions associated with cordons.

Integrating FEMA P-58 and Spatial Analysis of Cordons to Assess Building Functionality Throughout a Community

The proposed framework for assessing post-earthquake recovery of building functionality across a community is illustrated in Figure 2. The following sections provide an overview of each step in the process, details of which are described further in a case study application of the framework, presented later in the paper.

Community Functionality Model (Step 1)

Referring to Figure 2, the community functionality model describes the assets of the built environment that are necessary to support the desired community functions.

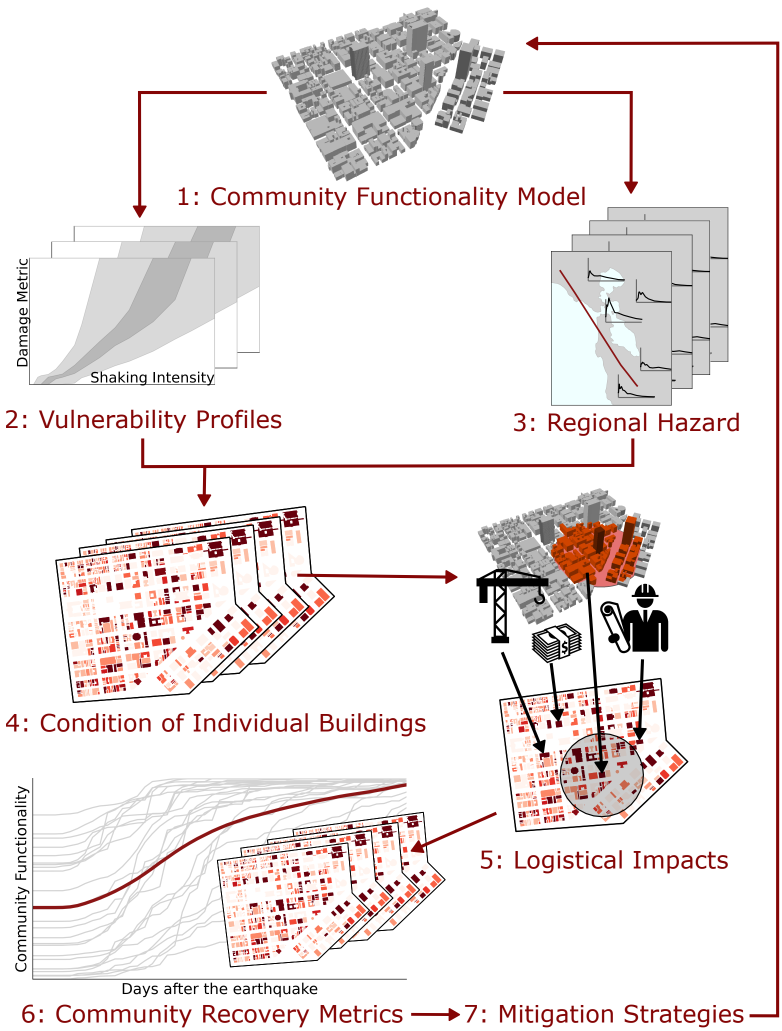

Figure 2. The primary steps of the proposed framework, with arrows denoting the flow of analysis and graphics illustrating key concepts at each step: (1) the community functionality model, (2) building vulnerability profiles and (3) ground motion maps for regional hazard are sampled to generate (4) realizations of each building's post-earthquake condition. The recovery process incorporates the (5) logistical impacts associated with building damage, impeding factors, and cordons. The suite of possible recovery trajectories for the community's functionality is distilled into summary (6) recovery metrics. These metrics can be used to evaluate (7) mitigation strategies that, in turn, influence the underlying community functionality model.

These functions typically relate to socioeconomic sectors, such as medical, educational, government, business, or retail services. The community functions are then associated with specific buildings in the community functionality model. Summaries of resilience objectives (e.g., Figure 1a) typically focus on whether these buildings can support their community services, such as the time until commercial office spaces re-open to support their function after an earthquake (SPUR 2009; NIST 2016). The factors that can impact building functionality will in turn determine which features are necessary to include in the community functionality model. For example, if the assessment focuses on the influence of building damage and cordon-related access restrictions on building functionality, then an inventory of the buildings is sufficient for the community model. If the assessment also considers closure due to loss of utilities or transportation access for employees to arrive on site, the community model should include the utility and transportation networks.

Vulnerability Profiles (Step 2)

The performance of each asset in the community functionality model is simulated via vulnerability profiles that contain many realizations of decision variables, DV, conditioned on a range of shaking intensities, IM. These stored realizations serve as probability distributions, $P(DV|IM)$. When considering building assets, each vulnerability profile is derived from a full FEMA P-58 analysis of the building response, component damage, and the resulting decision variables, i.e., the EDP, DM, and DV. In the following case study, the DVs include the building repair time (considering both the repairs required to restore functionality and, if necessary, the smaller subset of repairs required to stabilize the building—as described later in the case study), triggers for cordons, and triggers for other impeding factors.

Each building in the community inventory is associated with a unique vulnerability profile, which may represent individual buildings or a class of buildings, such as low-rise, concrete moment frame office buildings. Each profile is based on a building component model for simulating damage and consequences, $P(DV|DM)P(DM|EDP)$, and an underlying building analysis model for the building response, $P(EDP|IM)$. As each vulnerability profile is modeled independently, the level of complexity for the building analyses is flexible. This allows for applying detailed nonlinear response history analysis for tall buildings, for which damage can have more severe consequences for the community. In contrast, less influential buildings could be evaluated with simpler and less computationally intensive models at the discretion of the modeler (e.g., simpler analysis models for building response or Hazus-type building-level fragility functions).

Regional Hazard (Step 3)

Regional hazard is characterized by mapping realizations of ground motion shaking intensities, IM, for one or more earthquake scenarios. The maps reflect the variability in shaking intensities, including the spatial distribution of ground shaking across the region. The choice of intensity measures depends on the required input for the vulnerability profiles. Typically, the maps include spectral acceleration, $Sa(T)$ at one or more periods, T, for each location, but other parameters such as shaking duration could be included.

Ground motion IMs are typically determined using ground motion prediction equations, although direct simulations could also be used, similar to those in the HayWired Scenario (Wein and Detweiler 2018). Ground motion prediction equations provide the logarithmic means and standard deviations of spectral accelerations for a given location, using predictor parameters such as rupture magnitude, distance from the rupture, and site (near-surface soil) conditions. Related models quantify the spatial and across-period correlations of the spectral accelerations, considering both the between- and within-event variability in shaking intensities. Together, these means, standard deviations, and correlations are used to simulate a suite of unique realizations of ground motion intensity maps that collectively represent the probability of shaking, $P(IM)$, for an earthquake scenario.

Condition of Individual Buildings (Step 4)

Once the building vulnerability profiles and ground motion maps are prepared, they are used to sample the post-earthquake condition of each building in the community. For each ground motion map realization, intensity measures, e.g., $Sa(T)$, are sampled for each building location, considering any building specific parameters, e.g., the fundamental period, T. The intensity measure for each building is, in turn, used to sample a realization of decision variables (repair time, repair cost, etc.) from each building's vulnerability profile. For tall buildings, a cordon trigger index is also sampled. Depending on the definition of the cordon trigger, it may reflect the building's impaired collapse safety, damage to exterior cladding, or both.

Sampling many realizations of building conditions produces a full distribution of the potential damage across the community. The collection of realizations, sampled from the distributions for $P(DV|IM)$ and $P(IM)$, incorporates the uncertainty in ground shaking intensity measures (via the ground motion maps) and in the decision variables (via the vulnerability profiles). The individual building conditions for a given ground motion map realization are sampled independently, however the ground motion correlation does produce some correlation in building performance. By developing and storing the building vulnerability data and ground shaking maps in separate, parallel processes, any number of community realizations can be computed quickly for alternative earthquake scenarios, without recomputing the building-specific FEMA P-58 analyses.

Logistical Impacts (Step 5)

Having simulated the post-earthquake condition of individual buildings, the next step is to evaluate the logistical delays in the subsequent recovery process, due to cordons and other impeding factors. An impeding factor model is applied to each building to determine when repairs can be initiated. The model includes both REDi's impeding factors for individual building-level delays and the community-level impact of access restrictions due to a cordon around a nearby building. The cordon occurrence and location depends on the sampled condition of each tall building. If a cordon is triggered, it is assumed to remain in place until the damaged building is stabilized (e.g., the structural system and exterior cladding are repaired or the collapse/falling hazard is reduced via shoring).

The cordon duration is included in the impeding factor model for every neighboring building within the cordon. Both the duration and the extent of the cordon are informed by modeling assumptions, such as those applied in the case study described later. As procedures and protocols are developed for establishing and maintaining cordons, they can inform these assumptions (FEMA P-2055 2019). Once each building's impeding factor delay is evaluated, it is added to the functional repair time to obtain a total downtime for each building in the community.

Community Recovery Metrics (Step 6)

At this step, the downtimes of each individual building are aggregated to quantify the community functionality over time after the earthquake (e.g., the percent of commercial office space that is restored to its function). The number of buildings (and associated office space) that have been restored to functionality is computed at discrete time steps after the earthquake to create a recovery curve (Bruneau et al. 2003) for each realization. The recovery curves for all the realizations represent the probability distribution of the community performance. As illustrated in the case study presented in the next section, the distribution of recovery curves can be distilled into an expected (i.e., average) recovery curve, along with other scalar metrics of recovery.

Mitigation Strategies (Step 7)

The recovery metrics from the community assessment framework reveal the gap between the desired performance and the expected performance (Figure 1a). Strategies such as mandatory retrofits (to reduce damage by improving the building performance) or preparedness planning (to shorten the impeding factor durations) can mitigate the disruption due to the earthquake, reducing the gap. The community recovery metrics allow resilience planners to compare the various mitigation strategies based on multiple dimensions.

Illustrative Case Study: Downtown San Francisco

The proposed community recovery framework is applied to a case study to examine building damage and recovery in San Francisco's dense downtown area, considering the impact of cordons around damaged tall buildings on the recovery of neighboring buildings. The study illustrates details associated with implementing each step of the proposed framework, providing an example of how to address them. Finally, it culminates in a comparison of the relative benefits of mitigation efforts, such as preparedness planning or building retrofits.

Community Functionality Model (Step 1)

The case study focuses on one aspect of community functionality, specifically the functional office space available in the downtown financial district. Office space represents over half of the total building space in downtown San Francisco and one of the *Resilient City* recovery targets is to restore functionality for 50% of the office space within four months of a design level earthquake (SPUR 2009, see Figure 1a, above). Potential disruptions are defined here as damage to each individual building or access restrictions due to cordons around tall buildings. Based on this definition, a functional office building (NIST 2021) is one for which any building damage that hindered functionality has been repaired and any cordon restrictions, which would otherwise limit building access, have been lifted. Note that additional disruptions, such as damage to utilities, transportation networks, or other externalities, could be considered by including the relevant components of the built environment (e.g., electrical substations and underground networks). While these disruptions have a significant impact on functionality, they are outside the scope of this case study. Moreover, though it is recognized that business recovery is contingent on the recovery of employees' residential housing, this aspect is also outside the scope of the present study.

The community model encompasses the downtown region of San Francisco with a dense population of tall buildings (Figure 3a). Of the 1078 buildings in the study area, 87 are taller than $75m$, which is a "tall building" designation based on triggers in the building code (ASCE/SEI 7-16 2016). The case study only considers cordons around buildings taller than this height. Assuming that the cordon radius is equal to 1.5 times the building height (per ATC-20-1 2015), the cordons typically extend over the length of a city block or more from the damaged tall building. The inventory of buildings for the study area was derived from tax assessor, land use, and LIDAR datasets available at San Francisco's open source portal, dataSF.org. The building attributes include location, year of construction, height, occupancy type, building area, and structural system (i.e., the attributes that are required for creating the vulnerability profiles in Step 2). The data required significant merging, cleaning, and assumptions, particularly for inferring the structural system. As such, the inventory is a reasonable representation based on publicly available data, rather than a reliable description of every building in downtown San Francisco. (See Hulsey 2020, Appendix A for more details on the inventory.) The office buildings in the downtown region are shown in red in Figure 3b. These 445 office buildings comprise about 58% of the community's total building space, about half of which is located in 60 tall buildings (over $75m$). The rest of the space supports other community functions such as residential (16%), retail (14%), and hospitality (8%).

In addition to the building attributes, the community functionality model also includes assumptions about the preparedness plans for each building. The baseline case assumes the same plans for all the buildings, specifically that (1) the funding mechanism for repairs is private bank loans and (2) there are no contracts with engineering firms or contractors to ensure quick mobilization after the earthquake. These assumptions will inform the recommended distributions for sampling the impeding factor durations in Step 5.

Vulnerability Profiles (Step 2)

The vulnerability profiles, developed based on FEMA P-58 analyses for each building, were generated using the SP3 tool (https://sp3risk.com/). The tool infers the building strength, along with the first three periods and elastic mode shapes, based on building

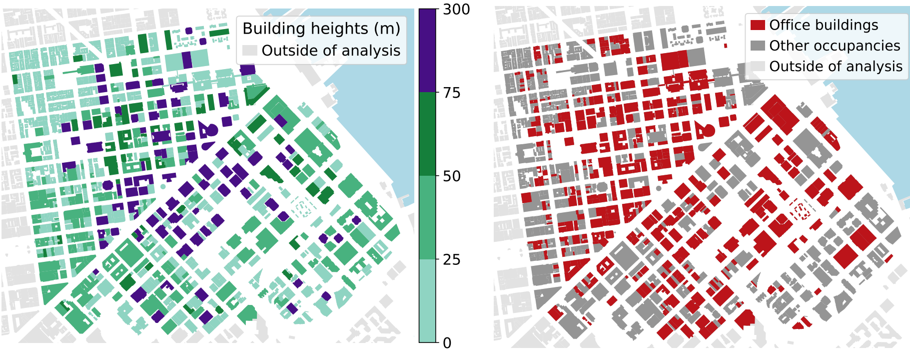

(a) (b)

Figure 3. Geographic extent of the case study and selected properties of the building inventory by **(a)** Building height, and **(b)** Building occupancy. Of the 1078 buildings in the region, 87 are over $75m$ tall and 445 are office buildings.

codes and typical design characteristics for a given structural system and year of construction. The elastic response parameters are adjusted, based on SP3's large database of response data for representative buildings, to generate expected drift and acceleration responses (EDP) over the height of each building, as a function of $Sa(T_1)$, where T_1 is the first period (Cook et al. 2018). Building component models are also compiled automatically, based on occupancy type, year of construction, and building dimensions. The EDP and component models are then used to perform the FEMA P-58 evaluation of building performance (Haselton 2018).

Each building in the inventory is associated with a unique vulnerability profile. Buildings with similar numbers of stories and structural systems will have similar EDP models but may have different component models based on the building function, total area, or story height. These and other variations between buildings could potentially be grouped together for one representative vulnerability profile; however, since the required computational effort was not prohibitive, this study uses unique vulnerability profiles for each building to avoid any assumptions required for consolidating the building inventory into groups.

As illustrated in Figure 4, the vulnerability profiles store the FEMA P-58 realizations for each building, representing the distribution of potential post-earthquake building conditions. The black tick marks in the figure represent individual realizations that were simulated at discrete shaking intensities, and the shaded regions represent probability percentiles. Note that for some intensities, a large percentage of the realizations are associated with building replacement, represented by coincident tick marks at the upper bound of the plot. This may be due to building collapse, residual drifts that render the building irreparable, or repair cost/times that exceed the equivalent resources required for replacement. The prevalence of such replacement cases explains why, visually, the cloud of tick marks appears to be inconsistent with the shaded percentile regions. Each vulnerability profile includes 5000 realizations to ensure an adequate resolution for the 1000 realizations of building damage that are sampled across the building inventory in Step 4 of the framework.

Each stored realization is characterized by the following decision variables: (a) the duration of the repairs required to restore building functionality (Figure 4a), (b) indicators of damage severity to inform the length of the impeding factor delays, and (c) repair cost as a fraction of the building replacement cost (Figure 4b). The duration for repairs and impeding factors are both based on REDi's functional recovery state, which corresponds to functional recovery as defined in a recent NIST-FEMA report (NIST 2021). For buildings over $75m$ tall, the realizations also include (d) a trigger for whether the building damage warrants a cordon, and (e) the duration of the repairs required for stabilizing the building. The stabilization duration is calculated as an alternate recovery state, similar to REDi's re-occupancy recovery state, which only considers significant damage. However, the stabilization recovery state is further limited to only include repairs of the structural components and exterior cladding that could jeopardize the safety of those around the building. The stabilization duration only applies if a cordon is triggered. Ideally, the cordon trigger(s) would be specific to the structural system and type of exterior cladding. Because the building-level decision variables are derived from a full FEMA P-58 analysis of the damage to each component, it is possible to incorporate any number of damage states or patterns as a cordon trigger (Hulsey 2020, Chapter 3). However, in the absence of detailed analysis for evaluating cordon triggers for each structural system, this case study uses peak story drift as an approximate cordon trigger for all tall buildings over $75m$. For buildings built before 2000, the trigger threshold is a peak story drift ratio greater than 2%. For buildings built after 2000, which are assumed to incorporate all the current detailing requirements for ductility, such as those introduced for reinforced concrete in the 1980s and for steel moment frames in the 1990s, the trigger threshold is 4% peak story drift.

Regional Hazard (Step 3)

This case study considers the earthquake scenario that is associated with the *Resilient City*'s recovery targets: a $M_w7.2$ on the San Andreas Fault, close to San Francisco (see the map in the upper left of Figure 5). The framework requires many realizations of regional hazard ground motion maps with shaking intensities at a set of locations and a range of spectral acceleration periods.

Each realization, k, simulates unique response spectra at each site, j, according to the following model:

$$\ln \boldsymbol{Sa(T)_{k,j}} = \mu_{\ln \boldsymbol{Sa(T)}_j} + \delta \boldsymbol{B_k} + \delta \boldsymbol{W_{k,j}} \tag{1}$$

where $\ln \boldsymbol{Sa(T)_{k,j}}$ is the logarithm of spectral acceleration (the bold text denotes a vector of spectral accelerations at a range of periods). The response spectrum spans all the building periods represented in the inventory, i.e., $0 \leq T \leq 6s$. The term $\mu_{\ln \boldsymbol{Sa(T)}_j}$ is the predicted logarithmic mean for the jth site, and $\delta \boldsymbol{B_k}$ and $\delta \boldsymbol{W_{k,j}}$ are the between- and within-event residuals, quantifying the kth realization's deviation from the mean.

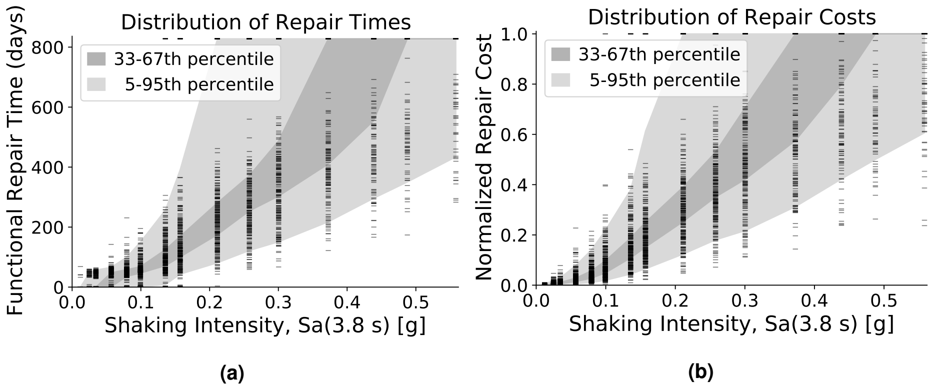

Figure 4. An example building vulnerability profile, containing realizations for the post-earthquake condition at a range of shaking intensities. Tick marks show individual realizations from FEMA P-58 analyses, and shading indicates percentiles of the distribution. **(a)** Duration of the repairs that are required for restoring building functionality **(b)** Repair cost, as a fraction of the building replacement cost.

The residuals $\delta \boldsymbol{B_k}$ and $\delta \boldsymbol{W_{k,j}}$ are simulated from zero-mean Gaussian random variables with standard deviations of $\boldsymbol{\tau}$ and $\boldsymbol{\phi}$, respectively. For a given realization, $\delta \boldsymbol{B_k}$ is constant for all sites, while $\delta \boldsymbol{W_{k,j}}$ varies with spatial correlation.

This case study uses the Chiou and Youngs (2014) ground motion prediction equation to obtain the logarithmic means ($\mu_{\ln \boldsymbol{Sa(T)}_j}$) and standard deviations (between- and within-event terms $\boldsymbol{\tau}$ and $\boldsymbol{\phi}$) that characterize the spectral accelerations at a particular location. The predictions are a function of rupture magnitude and the closest distance from the rupture to the site locations (approximately $13km$ for this case study). The ground motion maps are simulated for discrete reference sites roughly $1km$ apart, which is consistent with the spatial resolution of the ground motion prediction equation (i.e., at this distance from the fault, $1km$ would not significantly influence the median predicted intensity). The site locations are positioned to reflect the variation in soil conditions across the region (measured via average shear wave velocity over the top $30m$, V_{s30}). Ten reference sites are mapped in Figure 5. For three of the sites, the predicted median response spectra ($exp(\mu_{\ln \boldsymbol{Sa(T)}_j})$) and +/-1 standard deviation are displayed next to the map, shown in black and gray dashed lines, respectively.

For each realization, k, the simulation procedure incorporates both across-period and spatial correlations for the residuals. The between-event residual, $\delta \boldsymbol{B_k}$, has across-period correlation (among the periods, T, in the $\boldsymbol{Sa(T)}$ vector) but no spatial component, as it is constant across all sites. The within-event residuals, $\delta \boldsymbol{W_{k,j}}$, include both across-period and spatial (across-site) correlation, where sites that are close to each other are more likely to experience similar shaking than sites that are farther apart. These residuals are simulated using a computationally efficient correlation model (Markhvida et al. 2018), which takes seconds to generate residuals for 10,000 map realizations (more than

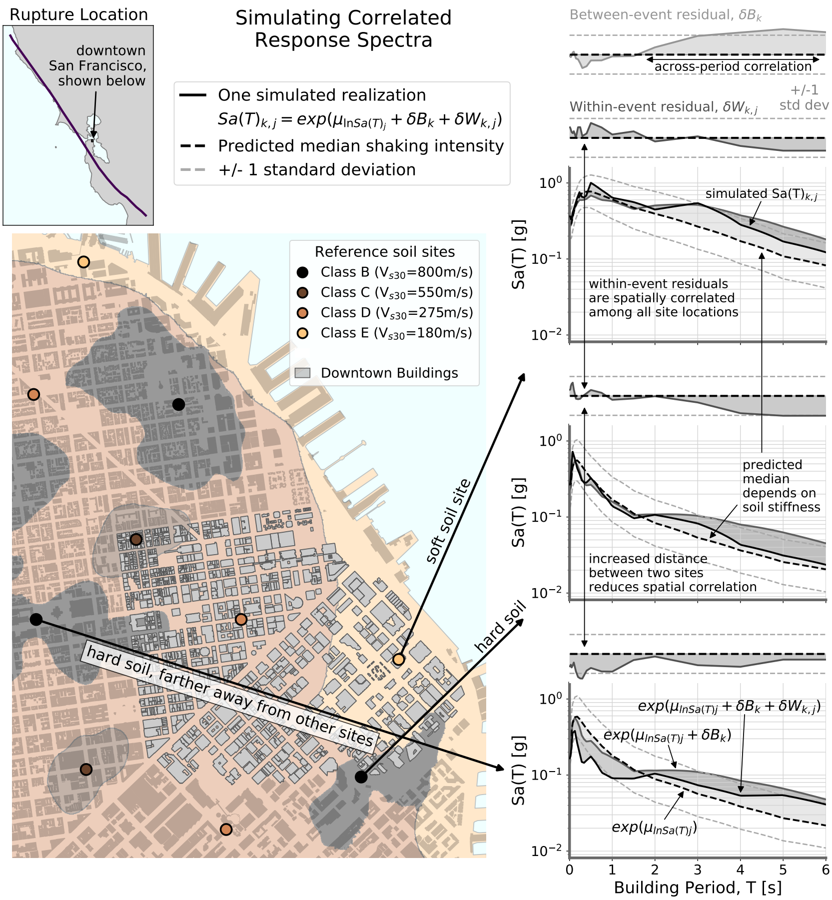

Figure 5. The components for simulating ground motion maps realizations, k, for a $M_w 7.2$ earthquake on the San Andreas Fault (upper left): $\boldsymbol{Sa(T)}$ response spectra are simulated for reference soil sites, j (colored circles on the map). The response spectra represent the shaking intensity for any nearby building situated on the same site class. The black dashed lines in the response spectra plots on the right show the predicted medians (exponent of the logarithmic mean, $\mu_{ln\boldsymbol{Sa(T)j}}$) for three reference sites, based on the location and soil condition (V_{s30}). The simulated between-event residuals ($\delta \boldsymbol{B_k}$, light gray in top right) incorporate across-period correlation and are consistent across all sites. The within-event residuals ($\delta \boldsymbol{W_{k,j}}$, the three darker gray plots) vary at each site and include both spatial and across-period correlations. Summing the mean and both residuals produces a response spectrum at each reference site, resulting in a single ground motion map realization. Visually, the gray solid lines in the spectral plots show (the exponent of) $\mu_{\boldsymbol{lnSa(T)j}}$ + $\delta \boldsymbol{B_k}$, while the solid black lines also include the location specific $\delta \boldsymbol{W_{k,j}}$.

sufficient for the 1000 community realizations that are used in Step 4). The simulated residuals are added to the logarithmic mean for each site to produce correlated response spectra, per Equation 1 and as shown in Figure 5's three site response spectra for one ground motion map realization. Together, the suite of ground motion maps collectively represent the estimated range of ground shaking in downtown San Francisco due to a $M_w 7.2$ earthquake on the nearby segment of the San Andreas Fault.

Condition of Individual Buildings (Step 4)

The building vulnerability profiles and the ground motion map realizations are combined to simulate the post-earthquake condition of each building. The case study includes 1000 community realizations, each based on one sampled ground motion map. For a given ground motion map realization, every building is assigned a spectral acceleration, $Sa(T)$, based on its fundamental period, T, and the nearest reference site in the same soil class. A realization of the building's condition is then sampled from the associated vulnerability profile, given the assigned input intensity measure. The black tick marks in Figure 4 show the distribution of realizations for functional repair times and the associated repair costs at each intensity level in the vulnerability profile. Given the similarity of adjacent distributions, the building condition is sampled from the nearest intensity, rather than interpolating between them. This avoids the challenge of correlated interpolation among the five decision variables that are sampled for each realization, i.e., a vector that includes the repair times and costs (shown in Figure 4), along with impeding factor indices and cordon triggers.

One of the important considerations in establishing the functional recovery time for buildings is determining the minimum damage threshold trigger for loss of functionality. While the REDi methodology considers this in the definition of the repairs that are required for the functional recovery state, REDi may overestimate the recovery time by ignoring steps taken to accelerate recovery for buildings with low levels of damage. While building closure typically results in long logistical delays (impeding factors) before functionality is restored (Comerio 2006), there is evidence indicating that the damage triggers for long-term building closure depend on the ingenuity of building owners/managers to alleviate the impact of damage that is straightforward to repair and does not require significant engineering interventions (Mitrani-Reiser et al. 2012; Jacques et al. 2014). Recent work has explored the damage threshold for building closure by differentiating between REDi's definition of the reoccupancy recovery state and the less conservative "shelter-in-place" associated with temporarily reduced habitability standards (Molina Hutt et al. 2021); however, this work is limited in scope to residential occupancies. In the absence of established models to account for these factors for office space, this case study assumes that a building with repair costs $\leq 10\%$ of the building replacement cost will remain functional after the earthquake, thereby alleviating the long logistical delays associated with a full building closure.

Once the post-earthquake condition of every building has been sampled, the impact of the cordons is evaluated. As noted previously, the number and location of cordons is based on the triggering condition of the tall buildings. The cordon size is based on a baseline assumption of a circular cordon with a radius equal to 1.5x the height of the building, as suggested in CALBO (2013) and ATC-20-1 (2015). The spatial analysis to determine which neighboring buildings are affected is based on the centroid of the building footprints. When a building is impacted by multiple overlapping cordons, the building access is restricted until the last remaining cordon is removed. Evaluating the cordon boundaries and the number of buildings that lie within the cordons for each realization of the community's post-earthquake condition provides a probabilistic estimate of the number of buildings affected by cordons. As shown in Figure 6a, there is a 50% chance of having at least 14 cordons or of having almost 400 buildings within the cordoned area (shown by the dashed lines that extend from the 50^{th} percentile of the corresponding histograms). As shown in Figure 6b, the median number of cordons (14) coincidentally results in a loss of about 50% of the office space. Note that the tall buildings that require a cordon also lie within the cordon and are therefore counted among the affected buildings. Due to the concentration of office space in the tall buildings, there is a 25% chance that over 85% of the office space will be affected by cordons (referring to the horizontal 75^{th} percentile line in Figure 6b).

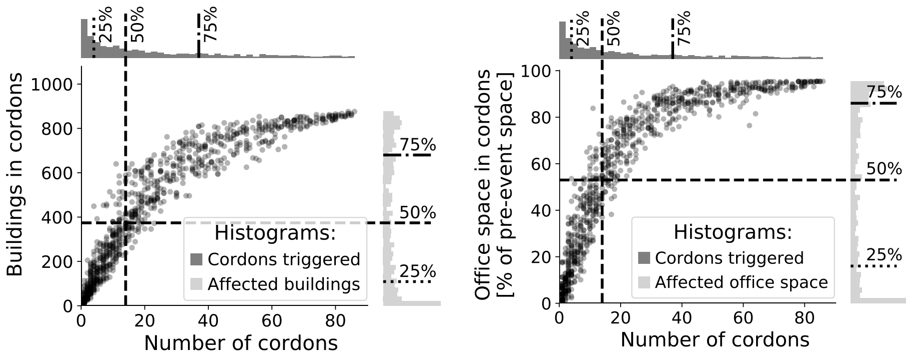

(a) **(b)**

Figure 6. The number of cordons required due to damage to tall buildings (x-axis) and their impacts (y-axis). The points in the scatter plot show all the community realizations, with histograms at the top and right representing the marginal distributions. The black lines in the histograms correspond to the 25^{th}, 50^{th}, and 75^{th} percentiles. **(a)** Number of buildings affected by the cordons. **(b)** Percentage of office space affected by the cordons.

Figure 6 further demonstrates one of the benefits of using high-resolution simulation to account for each building's spatial location and uncertain response. Each point in the scatter plots represents a transparent link between the simulated tall building damage and the resulting cordons for each community realization. For example, a realization with more cordons could be traced to a ground motion map with more intense shaking than the predicted median (perhaps due to a between-event residual, $\delta \boldsymbol{B_k}$, that is high for the long periods associated with tall buildings, as in Figure 5). Similarly, each building's sampled decision variable metrics (e.g., repair time and cost in Figures 4a and 4b) summarize the damage for a unique, internally consistent FEMA P-58 realization, rather than assuming a correlation model between fitted distributions of each metric.

Logistical Impacts (Step 5)

The logistical impacts (impeding factors) include both the delays due to the cordons and the conventional pre-repair delays from the REDi impeding factor framework. The duration of each cordon is the time it takes to stabilize the tall building that triggered it (see Step 2 for the description of this recovery state). Shown in Figure 7a is an example of how the cordon duration is calculated based on the stabilization repairs of a tall building that requires a cordon, and shown in Figure 7b is an example of neighboring buildings that are impacted by the cordon.

Referring to Figure 7a, for tall buildings that require cordons, it is assumed that the repair activity associated with removing the cordons can occur despite the access restrictions. Therefore, the repair begins as soon as the initial inspection and the parallel processes for financing, engineering/permitting, and contractor mobilization are resolved. The durations of each impeding factor are sampled from REDi's suggested distributions (see Table 8 in Almufti and Willford 2013), considering the amount of damage, the building height, the financing mechanism, and preparedness plans for securing engineers and contractors. The cordon is only necessary for the duration of the stabilization repairs for the structural system and exterior cladding, which is one of the metrics sampled from the vulnerability profile (see Step 2). Thus, for tall buildings that trigger a cordon, the duration of the cordon (e.g., 40 weeks for the sampled realization in Figure 7a) is calculated as the maximum impeding factor duration plus the stabilization repair time, while the total recovery time (e.g., 53 weeks) includes the additional time for the remaining functional recovery repairs.

As illustrated in Figure 7b, the cordon durations are included as impeding factors for buildings within the cordon radius. Specifically, the cordon delay is treated as a fourth parallel impeding factor that needs to be resolved prior to initiating repairs (see Hulsey 2020, Appendix C for a discussion of more complex interactions). A cordon that lasts longer than the maximum impeding factor would induce additional downtime for the building by postponing the initiation of repairs. This figure shows REDi's recommended median impeding factor durations for a standard (non-high-rise) building with significant damage, the baseline impeding factor assumption (no special preparedness plans), and the 40-week cordon duration from Figure 7a.

Once the duration of each building's recovery phases (impeding factors, the cordon delay, and repairs) have been established, they are aggregated to quantify the recovery of the community's office space over time. Figure 8 represents one simulated community realization with 14 cordons (which can be traced to one of the points on the vertical line for the median number of cordons in Figure 6a). While Figure 6a demonstrated the spatial impact of cordons immediately after the event, Figure 8 maps the recovery status of each building in the community at 4 and 12 months after the earthquake. Blue buildings are still waiting for their own impeding factors to be resolved prior to initiating repairs, while repairs to the orange buildings are further delayed by the cordons. Once both the

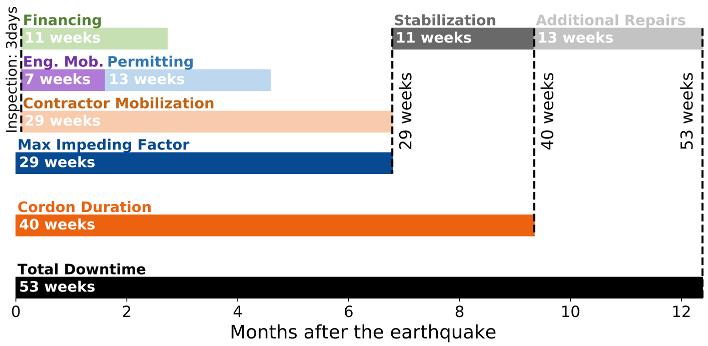

(a) A damaged tall building that requires a cordon

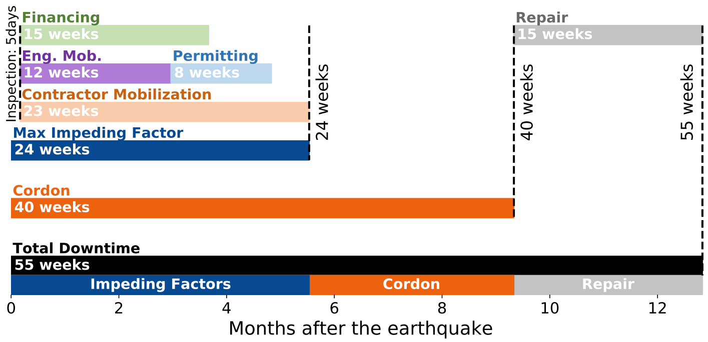

(b) A neighboring building affected by the cordon

Figure 7. Chart of the recovery activities for an individual building. **(a)** *A damaged tall building that requires a cordon*, where building stabilization repairs begin after the impeding factors are resolved. The cordon is removed after the building is stabilized, while additional repairs continue prior to reopening the building. (The durations of each impeding factor and the repair times are taken from a sampled realization for one of the tall buildings.) **(b)** *A neighboring building affected by the cordon*, where repairs are not initiated until the cordon is removed, even if the impeding factors have been resolved. (The durations depict REDi's recommended medians for significant damage to a non-high rise building that does not carry insurance or contracts with engineers or contractors, along with the cordon duration from 7a.)

impeding factors and any cordons are resolved, the repairs are initiated (gray) until the building functionality is restored (green). At 4 months, the recovery delays are dominated by the conventional impeding factors. The impact of the cordons is more apparent at 12 months, when the affected buildings' other impeding factors have been resolved yet repairs cannot be initiated until the cordons are removed. (Note that Figure 8 shows only one realization and does not quantify general patterns of cordoning, but serves to illustrate the type of information that the approach provides.)

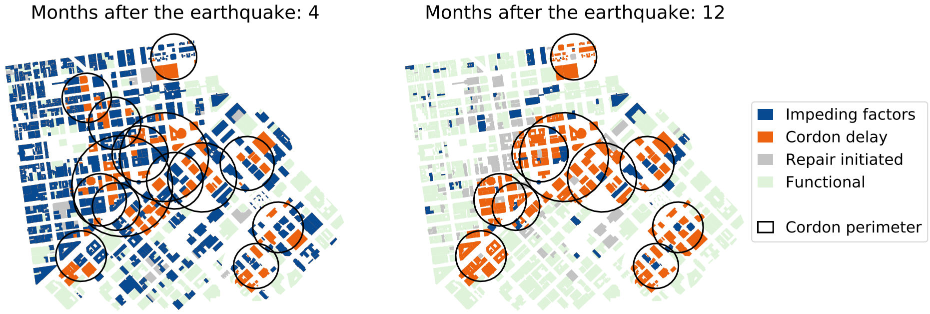

Figure 8. Maps of one recovery realization, showing the status of each building in the case study area at 4 months and 12 months after the earthquake. Blue buildings are still waiting for their own impeding factors to be resolved prior to initiating repairs, while orange buildings are further delayed by the cordons. Once both the impeding factors and any cordons are resolved, the repairs are initiated (gray) until the building functionality is restored (green). This realization includes 14 cordons (the median number across all realizations).

Community Recovery Metrics (Step 6)

While the community recovery can be mapped at discrete times for any one realization, it is also useful to consider summary statistics for the full distribution of all the possible recovery trajectories. A recovery curve depicts the community functionality over time, with a functionality metric on the vertical axis and time on the horizontal. Figure 9a shows a recovery curve for commercial office space within the downtown area, relative to the pre-event capacity. Each gray line is one realization, showing how much of the total available office space is still functional after the earthquake (the initial drop from 100%) and how quickly it recovers over time. The area above each curve is equivalent to the total loss of functionality for that realization (Bruneau et al. 2003). For clarity, the figure only shows every 33rd realization, for a total of 30 of the case study's 1000 realizations. The distribution of the realizations reflects the variability in both the ground motions and the building vulnerabilities that are incorporated within the analysis. As shown in Figure 9a the variability is significant, where the initial loss in office space ranges from nearly 0% to 100% for the scenario earthquake. To explore the relative impact of variability in the ground motion maps versus the vulnerability profiles, the results are recomputed and shown in Figure 9b based on the median predicted shaking intensity, i.e., with ground motion variability removed. Comparing the results, the median recovery curves (dashed lines in 9a and 9b) are similar, whereas the variability is much less. Due to differences in the magnitude and skew of the probability distributions, the expected (average) recovery curves are different.

The recovery curve realizations can be used to calculate scalar metrics to facilitate comparisons between assessment cases. One such metric is the functionality loss in the first year, which corresponds to the shaded gray region above the expected recovery

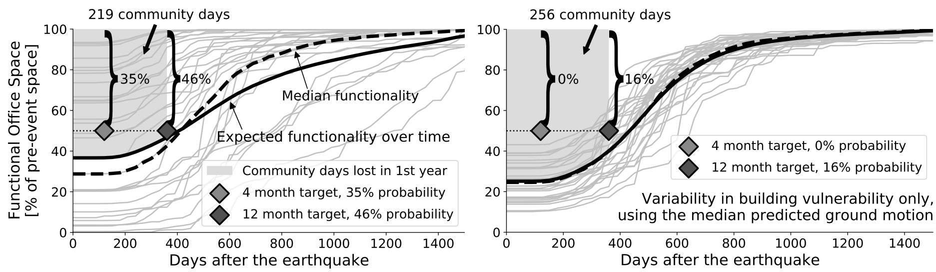

(a) **(b)**

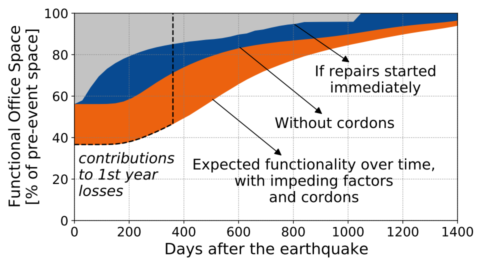

(c)

Community days lost in the 1st year	219
Repair	90
Impeding factors	54
Cordons	75
Probability of 50% functionality in	
4 months	35%
12 months	46%

(d)

Figure 9. Community recovery metrics, based on recovery curves for the accessible office space over time. **(a)** Recovery metrics for the baseline case. The gray lines are a subset of the 1000 realizations in the case study. The solid black line shows the expected (average) functionality and the dashed line is the median. The shaded gray area above the expected functionality is the number of community days lost during the first year. The diamonds show the four and 12 month recovery targets for achieving 50% functionality. The percentage of realizations above each diamond represents the probability of achieving the target (35 and 46%, respectively). **(b)** Recovery curve realizations if the ground motion variability is not included (i.e., using the median predicted shaking intensity for each simulation).
(c) Disaggregation of the expected community days lost, due to repair time only (gray), the impeding factors (blue), and cordons (orange). **(d)** Summary of metrics from 9a and 9c.

curves (solid lines) in Figures 9a and 9b, calculated over the first 365 days after the earthquake. For the baseline results in Figure 9a, this equates to 219 community days lost in the first year, which is almost two-thirds of the yearly capacity. For comparison, the expected loss in Figure 9b, which does not include ground motion variability, is 256 community days lost (about 16% higher). (An inverse analysis, not shown here, considered ground motion variability in conjunction with each building's median vulnerability. The resulting expected loss was 176 community days.) Another metric is the probability of achieving a specified functionality level by a target date, such as the *Resilient City* target of 50% functionality at 4 months after the earthquake, see Figure 1a. Referring to 9a, 35% of the gray recovery curve realizations lie above the light gray diamond, representing 50% functionality at 4 months, which corresponds to a 35% probability of achieving this target. Extending the target to 12 months (dark gray diamond) increases the probability of achieving the target to 46%. As shown in Figure 9b, these metrics are drastically distorted when the ground motion uncertainty is not accounted for, where the corresponding probabilities of achieving 50% functionality would be 0% and 16% at 4 and 12 months, respectively. (For the inverse case with no uncertainty in the building response, the percentage of functional office space would still range from 0-100%, as in Figure 9a, but the 4 and 12 months probabilities of 50% functionality increase to 53% and 62%, respectively.)

In Figure 9c, the expected (average) loss of office space is disaggregated into the contributions from building repairs (gray area), conventional impeding factors (blue area), and the cordons (orange area). Here, the recovery curve formed by the boundary between the gray and blue areas considers only repair time, as though all repairs began immediately after the earthquake. The curve between the blue and orange includes the additional delays due to impeding factors, and the curve at the bottom of the orange region includes delays due to cordons (equivalent to the solid black recovery curve in Figure 9a). Using the colored areas, the expected number of community days lost in the first year can be attributed to the underlying contributors. As summarized in the table in Figure 9d, of the 219 community days lost in the first year, about 41% are attributed to building repairs, 25% to conventional impeding factors, and 34% to the cordons. The 50% recovery probabilities are also included in the table. Having established these metrics, it is possible to compare the baseline case to any number of mitigation strategies or sensitivity analyses, as in the next section.

Mitigation Strategies (Step 7)

A key motivation for developing the proposed framework is to inform resilience planning by quantifying the anticipated recovery for the status quo and the effectiveness of mitigation strategies to accelerate the recovery. Figure 10 includes an enumerated list of the assessment cases considered. The baseline case (#1, as described in the previous sections) includes no preparedness plans for mitigating the impeding factor durations and a cordon radius of 1.5x the height of the building. Two sensitivity studies (#2-3) demonstrate the impact of the cordons extents, either by neglecting the cordons entirely or by reducing their radius to 1.0x the building height. Four cases examine alternative preparedness measures for tall buildings (#4-7), including alleviating the durations for contractor mobilization, engineering mobilization, financing, or all three. The impeding factor parameters for the preparedness plans are per the REDi recommendations (Table 1). (Note that while REDi also includes mitigation for the inspection time, it is only the order of days, rather than weeks, so it is not included here.) Another mitigation strategy (#8) focuses on employing seismic retrofits to reduce the vulnerability of older (pre-2000) tall buildings. Two final sensitivity studies (#9-10) consider the impeding factor durations - reducing them by 50% for all buildings, or eliminating impeding factor delays prior to the stabilization repairs for tall buildings that trigger cordons. Figures 10a-d show the full downtime disaggregation for four cases, while Figures 10e and f compare the scalar metrics for all ten.

Table 1. The impact of preparedness planning on the sampling distributions for the impeding factor durations associated with financing, engineering mobilization, and contractor mobilization. For brevity, the median and log standard deviation are only shown for cases with significant damage. (See Almufti and Willford 2013, Table 8 for additional values.)

Impeding Factor	Mitigation	Median (weeks)	Log standard deviation
Financing	Loans	15	0.68
	Insurance	6	1.11
Engineering	-	12	0.40
Mobilization	On contract	4	0.54
Contractor Mob.	-	40	0.31
(for ≥20 stories)	On contract	7	0.35

The results indicate that cordons contribute significantly to downtime across the community. As noted previously, in the baseline case (#1), 34% of the 219 community days lost in the first year are attributed to the presence of cordons (Figure 10a and e). As such, resilience planning efforts that do not consider the potential for cordons would significantly over-estimate the probability of achieving the 4- and 12-month recovery targets (see Figure 10f, case #2 versus #1). Case #3 considers the potential impact of further research into debris patterns, which could help mitigate community losses by supporting less conservative cordoning procedures. As seen by the disaggregation in Figure 10b, reducing the cordon radius from 1.5x to 1.0x the height of the building alleviates the number of undamaged buildings with access restrictions. Referring to Figure 10e and f, case #3 versus #1, the change in radius results in a moderate reduction in community days lost and improved probabilities for reaching the 50% occupancy targets.

One set of mitigation strategies is for tall building owners to undertake preparedness plans for reducing the impeding factor durations. Reducing the impeding factors for the tall buildings has two potential benefits: (1) any necessary stabilization repairs can be initiated sooner, decreasing the duration of the cordon for the neighboring buildings and (2) the functionality repairs are also addressed more quickly, restoring functionality to the tall buildings that contain the majority of the community's office space. Figure 10c shows the impact of adopting all of the preparedness measures (case #7). The results show that the contractor mobilization (case #4) makes the greatest impact, although the aggregate improvements in community days lost and the 4-month recovery probabilities are fairly modest, even when all three measures are taken (compare case #7 to #1). This suggests that damages always incur an impeding factor time cost that cannot be mitigated at the 4-month time scale. On the other hand, the combined mitigation measures are shown to improve the probabilities of achieving the 12-month recovery target from about 46% to about 58% (compare case #7 to #1 in Figure 10f).

A more aggressive and costly mitigation strategy is to retrofit the older (more vulnerable) tall buildings before an event (case #8), resulting in less initial loss of office space and fewer unstable buildings that require cordons (Figure 10d). The impact of retrofits are modeled by adjusting the building vulnerability profiles, using the same building attributes but revising the year of construction to reflect a building that satisfies

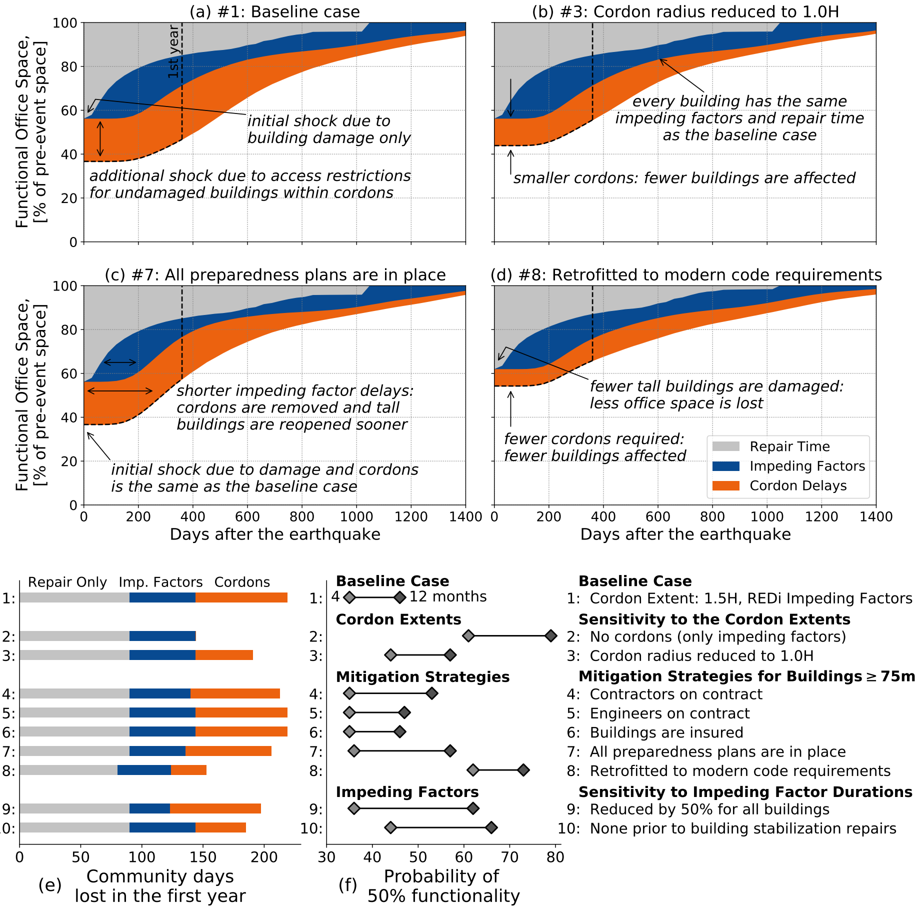

Figure 10. Comparisons of recovery metrics under the considered mitigation strategies: **(a)** Expected recovery curves for the baseline assessment case. Gray represents the loss of function due to repair time, blue is the marginal loss due to impeding factors, and orange is the marginal loss due to cordons. **(b)** Smaller cordon extents reduce the loss due to cordons. **(c)** Contingency planning mitigates the losses due to both impeding factors and cordons. **(d)** Retrofitting the tall buildings mitigates the losses from all downtime contributions. **(e)** The horizontal bars show the expected community days lost in the first year, per downtime contribution. **(f)** The light and dark gray diamonds show the probability of achieving 50% functionality at four and twelve months, respectively.

modern (post-2000) design requirements. The vulnerabilities are updated for the 79 tall buildings that were constructed before 2000 (out of a total of 87 tall buildings). As a result, the retrofits reduce the median number of cordons required from 14 (in the baseline case) to 2.

Based on the expected number of community days lost in the first year (Figure 10e), the seismic retrofits (case #8) have a clear advantage over the baseline (case #1) and other preparedness planning (case #7). Retrofitting reduces the loss by 66 community days, whereas the combination of all three preparedness plans only mitigates 13 community days. Referring to Figure 10f, the tall building retrofit option provides significant improvements in both the 4-month and 12-month targets, which are similar to the sensitivity study for eliminating the cordons altogether (case #8 versus cases #2 and #1). However, seismic retrofits are costly and take years to implement, while mitigation strategies based on preparedness planning can be established relatively quickly. Comparing the efficacy of preparedness plans versus seismic retrofit on the 12-month recovery probabilities (case #8 to #7 in Figure 10f), the retrofit still does better but the difference is not as compelling as for the 4-month target or the community days lost. Therefore, the perceived effectiveness of various mitigation strategies depends on the recovery target time frame and the priorities of the decision makers. Any policy decisions should consider the time and cost required to implement each option.

The final sensitivity studies probe the impact of reduced impeding factors, either by reducing the impeding factor durations by 50% for all buildings or by eliminating the impeding factors entirely prior to stabilization repairs for damaged tall buildings (cases #9 and #10). As with the preparedness planning for tall buildings (case #7), even a 50% reduction for impeding factor durations across all buildings (case #9) has a negligible impact on the probability of achieving the 4-month recovery target (Figure 10e). Eliminating the impeding factors prior to stabilization repairs (case #10) provides modest improvements, on the order of reducing the cordon radius to 1.0x the height of the building (case #3). In contrast, the reductions are more effective at improving the probabilities of achieving the 12-month recovery targets, almost to the level achieved by the tall building retrofit (probabilities of 66% and 62% for cases #10 and #9 versus 73% for case #8). Eliminating the impeding factors for the stabilization of damaged tall buildings is arguably among the most attractive options, since (1) it is less costly than the retrofit option, (2) it is probably more feasible to deploy resources for stabilization repairs on the cordoned buildings than to reduce the impeding factors and accelerate functional repairs on all the tall buildings simultaneously, (3) it reduces disruption and improves recovery trajectories of nearby buildings, and (4) the shorter stabilization time would minimize access disruptions to nearby roads. However, the experiences from Christchurch suggest that serious planning is needed to implement the strategy of eliminating (or significantly reducing) impeding factors for stabilizing tall buildings. For example, even when the Canterbury Earthquake Recovery Authority (CERA) was authorized to make unilateral decisions for the sake of accelerating community recovery, the process of stabilizing or demolishing buildings took on the order of eight months (Tombleson et al. 2018). While the circumstances in New Zealand were unique, including the local political/legal landscape and the impact of New Zealand's high insurance penetration rates, the experience demonstrates that such coordination is possible but would benefit from pre-event, community-level, interdisciplinary preparation.

Conclusion

The proposed framework for assessing the recovery of community functionality is intended to support seismic resilience planning for timely restoration of community functions after an earthquake. By utilizing high-resolution (building-parcel resolution) simulations with state of the art building performance models, the methodology allows for assessing community recovery trajectories based on distinct features and mitigation strategies at the individual building and community levels. In particular, the proposed framework accounts for the impact of cordons around damaged buildings in a dense downtown area, which can significantly affect the recovery trajectory.

The framework employs high-resolution post-earthquake recovery simulation, based on building-level performance assessments (FEMA P-58 and REDi), to model the impact of cordons on community recovery over time. The framework assesses building vulnerabilities and ground motion maps independently, then integrates the two for sampling multiple realizations of building damage and the required repairs. Once the post-earthquake building conditions across the community are sampled for each realization, the community functionality is tracked over time, considering the logistical delays that impact each building. The impacts include both conventional impeding factors for building repairs, such as the engineering/permitting process, and access restrictions due to cordons around heavily damaged buildings. Finally, the recovery realizations are distilled into community recovery metrics, including the expected number of community days lost in the first year (which can also be disaggregated into the contributions from cordons, impeding factors, or repairs) and the probability of achieving specified recovery targets (e.g., recovery of 50% of office space within 4 or 12 months of an earthquake).

A case study demonstrated the application of the framework by considering the functionality of office space in downtown San Francisco, following a $M_w 7.2$ earthquake on the San Andreas Fault. The results show that cordons are responsible for 75 (about one-third) of the expected 219 community days of office space lost in the first year. This indicates the importance of considering potential cordons when developing resilience plans and recovery targets. Sensitivity studies demonstrate the importance of capturing the variability in recovery curves, considering uncertainties in both the ground motion shaking intensity and the building vulnerability models. The community metrics produced by this framework facilitate evaluations of various mitigation strategies such as building retrofit mandates or preparedness planning to speed recovery. The metrics also distinguish between strategies that are effective for achieving short-term versus longer-term recovery targets. In addition to the mitigation strategies, sensitivity studies are used to examine which factors control the community recovery. This provides insight for areas of further research and in developing other mitigation strategies.

The case study was intentionally simplified in some ways for the purpose of demonstrating the framework. Three priority areas for further refinement include: (1) including building-specific data (in contrast to the data compiled from tax assessor and land use data) for the tall buildings for improved structural analysis models that better reflect their nonlinear response to strong ground motions and damage indicator thresholds that correspond to increased collapse vulnerability and cordon triggering, (2) improved models for logistical impacts on recovery times, including the impact of a cordon on transportation systems, demand surge, and resource limits, and (3) the spatial interaction between cordons, such as the impact of street patterns and the progression of stabilization repairs throughout the restricted area (the importance of this feature increases with the number of buildings that could require a cordon, as would occur if the model considers cordons around buildings less than $75m$ tall). Other extensions could be incorporated as research develops, such as considering liquefaction in the ground motion maps and vulnerability profiles or incorporating correlations when sampling building performance. Additionally, the practical application of the framework could be enhanced by an interface for interrogating the simulated results, such as identifying the cordon impact on critical functions (e.g., utility distribution centers or transportation hubs) or creating table top exercises for examining recovery strategies (e.g., priorities for building stabilization). However, even without such refinements and extensions, this framework offers important insights into the potential for cordons and promotes a better understanding of how to minimize their impact.

Supplemental material

The Python packages used in this recovery simulation, *cranes* and *seaturtles*, can be installed from the Python Package Index (PyPI) with examples at github.com/annehulsey/cranes and /seaturtles. *cranes* implements the steps of the framework (**C**ordons in **R**ecovery **A**ssessments of **N**eighborhoods following **E**arthquake **S**imulations). *seaturtles* simulates ground motion maps (**S**cenario **E**arthquakes **a**nd **t**he **U**ncertainty in **R**egional-**L**evel **E**stimates of **S**haking Intensities). The case study inputs and results are available at DesignSafe: doi:10.17603/ds2-dpam-dm40.

Acknowledgements

The first author would like to thank Adam Zsarnóczay for countless conversations on both the concepts of this framework and how to communicate them. Thanks also to Katie Wade of HBRisk and Wael Elhaddad of SimCenter for support in developing the vulnerability profiles and ground motion maps, respectively. Feedback from Francisco Galvis and Omar Issa enhanced the readability of this paper. This project was funded by Stanford University, the National Institute of Standards and Technology (NIST Award #70NANB17H245), and a FEMA graduate fellowship (awarded through the Earthquake Engineering Research Institute).

References

Adachi T and Ellingwood BR (2009) Serviceability assessment of a municipal water system under spatially correlated seismic intensities. *Computer-Aided Civil and Infrastructure Engineering* 24(4): 237–248. DOI:10.1111/j.1467-8667.2008.00583.x.

Almufti I and Willford M (2013) REDi Rating System: Resilience-based Earthquake Design Initiative for the Next Generation of Buildings. Technical report, ARUP, San Francisco, CA.

ASCE/SEI 7-16 (2016) *Minimum Design Loads and Associated Criteria for Buildings and Other Structures*. 7-16 edition. Reston, VA: American Society of Civil Engineers. ISBN 978-0-7844-0809-4. DOI:10.1061/9780784408094.

ATC-119 (2018) San Francisco Tall Buildings Study. Technical report, Applied Technology Council, Redwood City, CA.

ATC-20-1 (2015) Field Manual: Postearthquake Safety Evaluations of Buildings (2nd Edition). Technical report, Applied Technology Council, Redwood City, CA.

Bruneau M, Chang SE, Eguchi RT, Lee GC, O'Rourke TD, Reinhorn AM, Shinozuka M, Tierney K, Wallace WA and von Winterfeldt D (2003) A Framework to Quantitatively Assess and Enhance the Seismic Resilience of Communities. *Earthquake Spectra* 19(4): 733–752. DOI: 10.1193/1.1623497.

Burton HV and Deierlein GG (2018) Integrating visual damage simulation, virtual inspection, and collapse capacity to evaluate post-earthquake structural safety of buildings. *Earthquake Engineering & Structural Dynamics* 47(2): 294–310. DOI:10.1002/eqe.2951.

Burton HV, Deierlein GG, Lallemant D and Lin T (2016) Framework for Incorporating Probabilistic Building Performance in the Assessment of Community Seismic Resilience. *Journal of Structural Engineering* 142(8). DOI:0.1061/(ASCE)ST.1943-541X.0001321.

Burton HV, Deierlein GG, Lallemant D and Singh Y (2017) Measuring the Impact of Enhanced Building Performance on the Seismic Resilience of a Residential Community. *Earthquake Spectra* 33(4): 1347–1367. DOI:10.1193/040916EQS057M.

CALBO (2013) CALBO's Interim Guidance for Barricading, Cordoning, Emergency Evaluation and Stabilization of Buildings with Substantial Damage in Disasters. Technical report, California Association of Local Building Officials, San Francisco, California.

Carpenter LD, Naeim F, Lew M, Youssef NF, Rojas F, Saragoni GR and Adaros MS (2011) Performance of tall buildings in Viña del Mar in the 27 February 2010 offshore Maule, Chile earthquake. *The Structural Design of Tall and Special Buildings* 20(1): 17–36. DOI: 10.1002/tal.672.

CERA (2016) Public Geospatial Data: Christchurch Cordons Through Time. URL `https://ceraarchive.dpmc.govt.nz/documents/public-geospatial-data`.

Chang SE, Taylor JE, Elwood KJ, Seville E, Brunsdon D and Gartner M (2014) Urban Disaster Recovery in Christchurch: The Central Business District Cordon and Other Critical Decisions. *Earthquake Spectra* 30(1): 513–532. DOI:10.1193/022413EQS050M.

Chiou BSJ and Youngs RR (2014) Update of the Chiou and Youngs NGA Model for the Average Horizontal Component of Peak Ground Motion and Response Spectra. *Earthquake Spectra* 30(3): 1117–1153. DOI:10.1193/072813EQS219M.

Cimellaro GP, Arcidiacono V and Reinhorn A (2018) Disaster Resilience Assessment of Building and Transportation System. *Journal of Earthquake Engineering* DOI:10.1080/13632469.2018.1531090.

Comerio MC (2006) Estimating Downtime in Loss Modeling. *Earthquake Spectra* 22(2): 349–365. DOI:10.1193/1.2191017.

Contreras D, Blaschke T, Kienberger S and Zeil P (2014) Myths and realities about the recovery of L'Aquila after the earthquake. *International Journal of Disaster Risk Reduction* 8: 125–142. DOI:10.1016/j.ijdrr.2014.02.001.

Cook D, Wade K, Haselton C, Baker JW and DeBock DJ (2018) A structural response prediction engine to support advanced seismic risk assessmeng. In: *11th U.S. National Conference on*

Earthquake Engineering. Los Angeles, California.

Deierlein GG, Yen WY, Hulsey AM, Galvis F, Baker JW and Hutt CM (2020) Safety of Tall Pre-Northridge Steel Frame Buildings and Implications on Cordoning and Recovery. In: *17th World Conference on Earthquake Engineering, 17WCEE*. Sendai, Japan.

EERI (2010) 8.8 Chile Earthquake of February 27, 2010. Technical Report June, Earthquake Engineering Research Institute.

FEMA (2012a) Hazus multi-hazard Loss estimation methodology, earthquake model, Hazus-MH 2.1 technical Manual. Technical report, Federal Emergency Management Agency, Mitigation Division, Washington, D.C.

FEMA (2012b) Seismic performance assessment of buildings FEMA P-58-1. Technical Report September, Applied Technology Council, Washington, D.C.

FEMA P-2055 (2019) Post-disaster Building Safety Evaluation Guidance - Report on the Current State of Practice, including Recommendations Related to Structural and Nonstructural Safety and Habitability. Technical report, Applied Technology Council, Redwood City, CA.

Haselton CB (2018) The SP3 Building-Specific Risk Model. *SP3 Webinar Training Series* URL `https://vimeo.com/281330362`.

Hulsey AM (2020) *The regional impact of post-earthquake safety decisions based on damage to tall buildings and elevated hazard due to aftershocks*. PhD Thesis, Stanford University. URL `https://purl.stanford.edu/nr843bk0882`.

Jacques CC, McIntosh J, Giovinazzi S, Kirsch TD, Wilson T and Mitrani-Reiser J (2014) Resilience of the canterbury hospital system to the 2011 Christchurch earthquake. *Earthquake Spectra* 30(1): 533–554. DOI:10.1193/032013EQS074M.

Jayaram N and Baker JW (2010) Efficient sampling and data reduction techniques for probabilistic seismic lifeline risk assessment. *Earthquake Engineering & Structural Dynamics* 39: 1109–1131. DOI:10.1002/eqe.988.

Lee R and Kiremidjian AS (2007) Uncertainty and correlation for loss assessment of spatially distributed systems. *Earthquake Spectra* 23(4): 753–770. DOI:10.1193/1.2791001.

Markhvida M, Ceferino L and Baker JW (2018) Modeling spatially correlated spectral accelerations at multiple periods using principal component analysis and geostatistics. *Earthquake Engineering & Structural Dynamics* 47(5): 1107–1123. DOI:10.1002/eqe.3007.

Marquis F, Kim JJ, Elwood KJ and Chang SE (2017) Understanding post-earthquake decisions on multi-storey concrete buildings in Christchurch, New Zealand. *Bulletin of Earthquake Engineering* 15(2): 731–758. DOI:10.1007/s10518-015-9772-8.

Mieler M and Mitrani-Reiser J (2018) Review of the State of the Art in Assessing Earthquake-Induced Loss of Functionality in Buildings. *Journal of Structural Engineering* 144(3): 04017218. DOI:10.1061/(ASCE)ST.1943-541X.0001959.

Miranda E (2020) Personal communication, based on decades of earthquake reconnaissance trips.

Mitrani-Reiser J, Mahoney M, Holmes WT, De La Llera JC, Bissell R and Kirsch TD (2012) A functional loss assessment of a hospital system in the Bío-Bío province. *Earthquake Spectra* 28(SUPPL.1): 473–502. DOI:10.1193/1.4000044.

Moehle J and Deierlein GG (2004) A framework methodology for performance-based earthquake engineering. In: *13th World Conference on Earthquake Engineering*. Vancouver, B.C. Canada.

Molina Hutt C, Vahanvaty T and Kourehpaz P (2021) An analytical framework to assess earthquake-induced downtime and model recovery of buildings. *Earthquake Spectra* In Review.

Naeim F, Lew M, Carpenter LD, Youssef NF, Rojas F, Saragoni GR and Adaros MS (2011) Performance of tall buildings in Santiago, Chile during the 27 February 2010 offshore Maule, Chile earthquake. *The Structural Design of Tall and Special Buildings* 20(1): 1–16. DOI: 10.1002/tal.675.

NIST (2016) Community Resilience Planning Guide for Buildings and Infrastructure Systems, Volume 1. In: *NIST Special Publication 1190-1*. National Institute of Standards and Technology. DOI:10.6028/NIST.SP.1190v1.

NIST (2021) Recommended Options for Improving the Built Environment for Post-Earthquake Reoccupancy and Functional Recovery Time. In: *NIST-FEMA Special Publication FEMA P-2090/NIST SP-1254*, January. Gaithersburg, MD: National Institute of Standards and Technology. DOI:10.6028/NIST.SP.1254.

Raghunandan M, Liel AB and Luco N (2015) Aftershock collapse vulnerability assessment of reinforced concrete frame structures. *Earthquake Engineering & Structural Dynamics* 44(3): 419–439. DOI:10.1002/eqe.2478.

Rojas F, Naeim F, Lew M, Carpenter LD, Youssef NF, Saragoni GR and Adaros MS (2011) Performance of tall buildings in Concepción during the 27 February 2010 moment magnitude 8.8 offshore Maule, Chile earthquake. *The Structural Design of Tall and Special Buildings* 20(1): 37–64. DOI:10.1002/tal.674.

Shepard RB, Wood PR, Berrill JB, Gillon NR, North PJ, Perry AK and Bent DP (1990) The Loma Prieta, California, Earthquake of October 17, 1989: Report of the NZNSEE Reconnaissance Team. *Bulletin of the New Zealand Society for Earthquake Engineering* 23(1). DOI: 10.5459/bnzsee.23.1.1-78.

Shrestha S, Orchiston C, Elwood K, Johnston D and Becker J (2021) To cordon or not to cordon: The inherent complexities of post-earthquake cordoning learned from Christchurch and Wellington experiences. *Bulletin of the New Zealand Society for Earthquake Engineering* 54(1): 40–48. DOI:10.5459/bnzsee.54.1.40-48.

SPUR (2009) The resilient city: defining what San Francisco needs from its seismic mitigation policies. Technical report, San Francisco Planning and Urban Research Association, San Francisco, CA. URL `https://www.spur.org/publications/spur-report/2009-02-01/defining-resilience`.

Tombleson ZW, Yeow TZ, Khakurel S, Dhakal RP and Dawson CJ (2018) Quantifying downtime due to building demolitions in Christchurch. In: *2018 New Zealand Society for Earthquake Engineering*.

Underwood G, Orchiston C and Shrestha SR (2020) Post-earthquake cordons and their implications. *Earthquake Spectra* (May). DOI:10.1177/8755293020936293.

Wein AM and Detweiler ST (2018) The HayWired Earthquake Scenario — Engineering Implications Scientific Investigations Report 2017 – 5013 – I – Q. Technical report, U. S. Geological Survey. DOI:https://doi.org/10.3133/sir20175013v2.

Wesson RL and Perkins DM (2001) Spatial correlation of probabilistic earthquake ground motion and loss. *Bulletin of the Seismological Society of America* 91(6): 1498–1515. DOI: 10.1785/0120000284.